JBC Papers in Press. Published on May 16, 2018 as Manuscript RA118.002187
The latest version is at http://www.jbc.org/cgi/doi/10.1074/jbc.RA118.002187

Ablation of *Sirtuin5* in the postnatal mouse heart results in protein succinylation and normal survival in response to chronic pressure overload

Kathleen A. Hershberger[1,2], Dennis M. Abraham[3], Juan Liu[1,2], Jason W. Locasale[1,2], Paul A. Grimsrud[1], and Matthew D. Hirschey[1,2,4]

[1]Duke Molecular Physiology Institute and Sarah W. Stedman Nutrition and Metabolism Center, Duke University Medical Center, Durham, NC 27701. [2]Department of Pharmacology and Cancer Biology, Duke University Medical Center, Durham, NC 27710. [3]Department of Medicine, Division of Cardiology and Duke Cardiovascular Physiology Core, Duke University Medical Center, Durham, NC 27710. [4]Department of Medicine, Division of Endocrinology, Metabolism, and Nutrition, Duke University Medical Center, Durham, NC 27710.

Running Title: Ablation of *Sirtuin5* in the postnatal mouse heart

To whom correspondence should be addressed: Matthew D. Hirschey, Duke Molecular Physiology Institute, 300 North Duke Street, Durham, NC 27701, Phone: 919-479-2315, Email: matthew.hirschey@duke.edu

Keywords: Sirtuin, protein acylation, proteomics, stress, cardiac hypertrophy

ABSTRACT

Mitochondrial Sirtuin 5 (SIRT5) is an NAD^+-dependent demalonylase, desuccinylase, and deglutarylase that controls several metabolic pathways. A number of recent studies point to SIRT5 desuccinylase activity being important in maintaining cardiac function and metabolism under stress. Previously, we described a phenotype of increased mortality in whole-body SIRT5KO mice exposed to chronic pressure overload compared to their littermate WT controls. To determine if the survival phenotype we reported was due to a cardiac-intrinsic or cardiac-extrinsic effect of SIRT5, we developed a tamoxifen-inducible, heart-specific SIRT5KO mouse model. Using our new animal model, we discovered that postnatal cardiac ablation of *Sirt5* resulted in persistent accumulation of protein succinylation up to 30 weeks after SIRT5 depletion. Succinyl proteomics revealed that succinylation increased on proteins of oxidative metabolism between 15 and 31 weeks post ablation. Heart-specific SIRT5KO mice were exposed to chronic pressure overload to induce cardiac hypertrophy. We found that, in contrast to whole-body SIRT5KO mice, there was no difference in survival between heart-specific SIRT5KO mice and their littermate controls. Overall, the data presented here suggest that survival in SIRT5KO mice may be dictated by a multi-tissue or prenatal effect of SIRT5.

Sirtuin 5 (SIRT5) is an NAD^+-dependent demalonylase (1, 2), desuccinylase (2), and deglutarylase (3) that resides primarily in mitochondria. Previous studies demonstrated that SIRT5 desuccinylase activity is important in maintaining cardiac function and metabolism in response to stress. In a model of ischemia-reperfusion injury, infarct size in SIRT5KO mouse hearts was greater than WT littermates (4). Additionally, SIRT5 depletion was detrimental to cardiac function at 39-weeks of age, with defects in cardiac fatty acid oxidation (5). Finally, we recently observed increased mortality and impaired oxidative metabolism in whole-body SIRT5KO mice, compared to WT littermates, with the stress of chronic pressure overload-induced cardiac hypertrophy (6). Each of these three studies on the role of SIRT5 in the heart performed succinyl proteomic measurements in WT and SIRT5KO heart tissue in order to identify enzymes and pathways potentially regulated by SIRT5. In all three studies, key pathways in mitochondrial metabolism including oxidative phosphorylation, TCA cycle, and fatty acid oxidation were identified

as regulated by SIRT5 given the increase in succinylation on many enzymes in these pathways with SIRT5 depletion (6). Together, these data suggest that SIRT5 is important in maintaining cardiac function by desuccinylating key enzymes in oxidative metabolism. While these studies suggest that SIRT5 has a cardio-protective role, whether the effect of SIRT5 is cardiomyocyte-specific or due to an effect of SIRT5 outside the heart remains unknown.

Most characterization of the physiological roles of mitochondrial sirtuins have been conducted in whole-body sirtuin KO mice, including our forgoing work on the role of SIRT5 in cardiac function (6). However, differing degrees of acetylation in SIRT3KO tissues (7) and malonylation and succinylation in SIRT5KO tissues (8) suggest that the roles of sirtuins may differ between tissues. More recently, understanding the tissue-specific effects of mitochondrial sirtuins has emerged as an important area of investigation in order to determine contribution of individual tissues to phenotypes described in germline depletion models. For example, whole-body SIRT3KO mice on a high-fat diet have accelerated development of obesity, insulin resistance, hyperlipidemia, and steatohepatitis (9). However, in a liver- or skeletal-muscle-specific SIRT3KO model (two tissues with strong influence on whole body metabolism), no metabolic differences when compared to WT controls were observed despite similar hyperacetylation profiles to the whole-body SIRT3KO model (10). Either a tissue beyond liver/skeletal muscle or a coordinated tissue response was responsible for the phenotypes observed in the whole-body SIRT3KO mouse. Another major phenotype in the whole-body SIRT3KO mouse is the development of spontaneous cardiac hypertrophy (11, 12). A recent study found this phenotype is recapitulated in a skeletal muscle and heart-specific SIRT3KO model (13). However, it is not yet known if this is exclusively an effect of SIRT3 in cardiomyocytes; indeed, SIRT3 has also been shown to play a direct role in fibrosis (14), a key component in the development of cardiac hypertrophy. Thus far, no studies have been published on the tissue-specific roles of SIRT4 or SIRT5. Thus, there is a need to develop tissue-specific sirtuin KO models in order to better understand the tissues contributing to the phenotypes revealed in whole-body KO models. To this end, we set out to determine if the phenotypes described in the whole-body SIRT5KO mouse under chronic pressure overload induced hypertrophy (6) were recapitulated in a heart-specific SIRT5KO mouse model.

A well-established experimental tool to knock out genes in an inducible and cardiomyocyte-specific manner is the α-MHC-MerCreMer mouse model. In this model, two mutated estrogen receptors (Mer) flank a Cre transgene located upstream of the cardiomyocyte-specific myosin heavy chain-alpha (α-MHC) promoter (15). This system requires delivery of tamoxifen to bind to the mutated estrogen receptors, translocate to the nucleus, and induce expression of Cre. One benefit of using an inducible system is that the gene can be depleted postnatally, circumventing problems with embryonic lethally or compensation during early development. However, a major caveat of this mouse model is Cre toxicity in the heart, as evidenced by heart failure with high amounts of tamoxifen (16), and transient inflammation and hypertrophy with lower doses of tamoxifen (17). Here, we present data on the development and characterization of an inducible cardiomyocyte-specific SIRT5KO mouse model. Further, we analyze the cardiac morphological and functional changes with chronic TAC and survey the succinylation profile in this novel mouse model.

RESULTS

Characterization of heart specific, tamoxifen inducible SIRT5KO mouse model—To test if the cardiac phenotypes observed in the whole body SIRT5KO mouse (6) were heart intrinsic, we developed a heart-specific, tamoxifen-inducible, SIRT5KO mouse model. To generate this mouse, we crossed $SIRT5^{fl/fl}$ (18) mice with αMHC-MerCreMer mice to generate littermates with the following genotypes: $SIRT5^{fl/fl}$; αMHC-$MerCreMer^{-/-}$ (hereto referred to as fl/fl) and $SIRT5^{fl/fl}$; αMHC-$MerCreMer^{+/-}$ (hereto referred to as fl/fl;MCM). Additionally, the floxed alleles were crossed out of this line to generate a second line of αMHC-$MerCreMer^{-/-}$ and αMHC-$MerCreMer^{+/-}$ mice to generate αMHC-$MerCreMer^{+/-}$ (hereto referred to as MCM) mice to control for Cre toxicity.

Two methods of delivering tamoxifen were tested to determine optimal SIRT5 depletion in the

heart. First, adult mice were fed a commercially available tamoxifen citrate diet (Envigo Tekland Diets, TD.130860) for 3 weeks. In a second method, tamoxifen was dissolved in corn oil and given to adult mice by oral gavage at a dose of 80mg/kg for three consecutive days. We found that with either method of delivery, depletion of SIRT5 took more than two weeks (Fig. 1). Feeding tamoxifen citrate for three weeks followed by two weeks of regular chow resulted in approximately 75% depletion of SIRT5 (Fig. 1*A-B*) while two weeks after the oral gavage regimen, we observed about 50% depletion of SIRT5 (Fig. 1*D-E*). Since expression of Cre in the heart has been shown to be toxic and results in an acute cardiomyopathy (17), we measured cardiac hypertrophy by calculating the ratio of heart weight to body weight at multiple time points throughout these pilot studies. Although there was only a small sample size at each time point (n=1 or 2), there were trends of increased hypertrophy in the fl/fl;MCM mice compared to the fl/fl mice after three weeks of the tamoxifen diet (Fig. 1*C*). This hypertrophy appeared to normalize after two weeks of regular chow following the tamoxifen diet. No differences in heart weight to body weight were observed between the fl/fl controls and fl/fl;MCM mice in the oral gavage pilot study (Fig. 1*F*). Finally, we used RT-qPCR to further measure transcript levels of *Sirt5* and markers of Cre toxicity including *Nppa* (*Anf*), *Nppb* (*Bnp*), and *Il6*. Although SIRT5 protein levels were not diminished until weeks after tamoxifen dosing, *Sirt5* transcript levels were depleted at earlier time points (Fig. 1*G*). Maximal depletion of *Sirt5* transcript levels occurred after two weeks of the tamoxifen diet (Fig. 1*G*, left panel) and one day after the oral gavage dosing regimen (Fig. 1*G*, right panel). Transcript levels of Cre toxicity markers were highest after three weeks of tamoxifen diet feeding or one day to one week post oral gavage dosing (Fig. 1*H–J*). In the tamoxifen diet pilot group, transcript levels of *Anf*, *Bnp*, and *Il6* returned to control levels after two weeks of regular chow feeding. *Anf* and *Bnp* remained elevated in the oral gavage pilot group two weeks post oral gavage dosing (Fig. 1*H–I*). Based on these data, we proceeded with optimization of the tamoxifen diet feeding regimen because greater depletion of SIRT5 was achieved and we predicted that a shorter time on the diet would be sufficient to achieve depletion of SIRT5 and would result in less Cre toxicity. In studies described below, tamoxifen diet was fed for 8-10 days and we observed decreased evidence of Cre toxicity (data not shown).

Given that SIRT5 is a protein lysine desuccinylase and that succinylation in the whole-body SIRT5KO heart is abundant, we looked at succinylation over time after tamoxifen-induced ablation of *Sirt5*. Adult female mice were fed a tamoxifen citrate diet for 10 days followed by a regular chow diet. Mice were sacrificed immediately after the tamoxifen diet regimen, and 3-, 6-, 12.5-, and 32.5-weeks after the tamoxifen diet regimen. Western blotting was used to analyze succinylation and SIRT5 protein expression in whole heart lysates. Interestingly, we found that it took several weeks for protein succinylation to accumulate to levels that were comparable to succinylation in the whole-body SIRT5KO mouse (Fig. 2*A-B*). Specifically, 32.5 weeks after depletion of *Sirt5*, succinylation in fl/fl;MCM mouse hearts was about 3-fold greater than succinylation in the fl/fl mouse hearts. Although this was the maximum succinylation achieved in this time course, the whole-body SIRT5KO mouse heart has an approximate 5.5-fold increase in succinylation over the WT control (6). Thus, it is possible that sites of lysine succinylation would continue to accumulate if the time course was taken past 32.5 weeks. Interestingly, SIRT5 protein appeared to be maximally depleted 3 weeks after the tamoxifen diet feeding regimen (Fig. 2 *C*). Together, these data show that in our heart-specific, inducible SIRT5KO mouse model, SIRT5 is depleted after 3 weeks on the tamoxifen diet, yet succinylation continues to increase for at least 30 weeks. This important finding provides a unique tool to assess the effects of SIRT5 ablation with varying degrees of protein lysine hypersuccinylation, which might allow us to disentangle effects of SIRT5 from effects of protein succinylation.

Heart specific SIRT5KO succinyl proteomics—To further explore the increase in protein lysine succinylation after *Sirt5* ablation, we performed succinyl-proteomics in the fl/fl and fl/fl;MCM mice at 15 weeks and 31 weeks post-tamoxifen diet feeding. From the previous time course experiment, we predicted that we would observe a small increase in protein succinylation in the fl/fl;MCM mice 15 weeks post-tamoxifen diet feeding and a large increase in protein succinylation

in the fl/fl;MCMC mice 31 weeks post-tamoxifen diet feeding. Investigation of the cardiac succinylome at these time points would allow us to determine how the cardiac succinylome landscape changed with time after *Sirt5* depletion. Immediately after weaning, fl/fl and fl/fl;MCM mice were fed tamoxifen for 8 days and then returned to a regular chow diet. One group of mice were sacrificed 15 weeks after tamoxifen-induced ablation of *Sirt5* (n=2 fl/fl and n=3 fl/fl;MCM) and a second group of mice were sacrificed 31 weeks after tamoxifen-induced ablation of *Sirt5* (n=2 fl/fl and n=2 fl/fl;MCM) (Fig. 3 *A*). The left ventricle of hearts were pulverized and processed at the same time for succinyl proteomics analysis using a workflow leveraging peptide labeling with Tandem Mass Tag (TMT) 10-plex reagents (ThermoFisher Scientific), immunoprecipitation with anti-succinyl lysine antibody (Cell Signaling Technologies), and nanoflow LC-MS/MS analysis on a Q Exactive Plus Orbitrap. See supporting information table for quantitative data on relative succinylpeptide and protein abundances.

First, we analyzed changes in the proteome with respect to time and genotype. Using the parameters of Log_2 FC $\geq$1 and an adjusted p-value $\leq$ 0.1 (Benjamini-Hochberg correction; 10% FDR), there existed only one significant change in the proteome. Esr1 (estrogen receptor) was significantly increased in the 15-week SIRT5KO, compared to 15-week WT control (Fig. 3*B*). Esr1 induction is due to the constitutive transgenic overexpression of mutated estrogen receptors under the control of the MHC promoter and is thus not an effect of *Sirt5* ablation. We interrogated the pathways represented in the top 5% (Fig. 3*B*; red) and bottom 5% (Fig. 3*B*; blue) of proteins when ranked according to fold change and found pathways that were significantly overrepresented in these groups. Among the proteins that increased the most in hearts with *Sirt5* ablation, the pathways of muscle contraction and response to stress were increased, while among the proteins that decreased the most in hearts with *Sirt5* ablation, pathways of muscle organ development, sensory perception of sound (an irrelevant pathway in heart), muscle contraction, and cellular component of morphogenesis decreased. Given that proteins in muscle contraction both increased and decreased, this is likely due to the fact that a large number of these proteins were identified in heart tissue. These pathways were also represented in a pathway analysis comparing the Log_2FC of SIRT5KO/WT 31 weeks post tamoxifen feeding (data not shown). Importantly, proteins in oxidative metabolism (the main targets of protein lysine succinylation) are not significantly changed with ablation of *Sirt5* in the heart.

Next, we compared the succinylome generated in the heart-specific SIRT5KO and the succinylome we previously generated from the hearts of whole body SIRT5KO mice (6). Given the different proteomic techniques and study designs, we expected to identify a smaller number of sites of succinylation in the heart-specific SIRT5KO succinylome compared to the whole body SIRT5KO heart succinylome. In the heart-specific SIRT5KO succinylome, we identified (at 1% FDR) and quantified 1,631 succinylated peptides (an additional 504 succinylated peptides were identified but not quantified) that mapped to 462 unique proteins (Fig. 3*C*). Interestingly, only about half of these succinylated peptides were also identified in the whole-body SIRT5KO heart succinylome. We ranked the identified succinylated peptides in descending order in both succinylome data sets, and found that of the top 50 peptides increased in the heart specific SIRT5KO compared to WT hearts 31 weeks post tamoxifen feeding, half were also in the top 50 peptides increased in the whole body SIRT5KO heart compared to WT heart (Fig. 3*D*; light blue shaded bars). Additionally, the top 50 succinylated peptides in the heart specific data set were all identified in the whole body SIRT5KO heart succinylome. Together, this comparison illustrates that the SIRT5 targets identified in these proteomic data sets had strong overlap—and the two models of SIRT5 deficiency have similar effects on the succinylome of the heart relative to their respective controls.

The goal of the current study was to determine how the protein succinylation landscape changes over time after SIRT5 depletion, specifically in the heart. To begin to answer this question, we performed pathway analyses on a group of peptides that had increased succinylation, compared both to their respective time control (KO/WT at 15 weeks and KO/WT at 31 weeks; Fig. 4*A–B*) and to their genotype control (KO 31 weeks/KO 15 weeks and WT 31 weeks/WT 15 weeks; Fig. 4*C*). We used parameters of Log_2 FC $\geq$1 and an adjusted p-value $\leq$ 0.1 (Benjamini-

Hochberg correction; 10% FDR) to make a list of proteins for each given comparison that had increased succinylation. These lists were uploaded to PANTHER to perform statistical over-representation tests (19) to determine pathways that were particularly susceptible to succinylation in this model. The top three significantly overrepresented pathways in each comparison (except WT 31 weeks/WT 15 weeks where we saw no change in protein succinylation) were fatty acid beta-oxidation, tricarboxylic acid cycle, and oxidative phosphorylation or cellular amino acid catabolic process. Together, these data suggest that proteins in the same metabolic pathways are succinylated in the SIRT5KO heart at 15 weeks and 31 weeks-post SIRT5 depletion; indeed, these pathways are significantly over-represented in this comparison (Fig. 4*D*). There were no peptides with changes in succinylation when comparing the succinylation profile of WT hearts at 15 and 31 weeks after tamoxifen feeding (data not shown), demonstrating that few changes in the sites of protein succinylation occur under basal conditions in this time frame.

We hypothesized that the increase in succinylation that occurs in the SIRT5KO heart between 15 and 31 weeks post SIRT5 depletion was due to either an increase in the number of unique sites of succinylation, or a further increase in succinylation at lysine residues already succinylated. The succinyl proteomics performed here does not allow us to fully address the former possibility due to the mutiplexed nature of our workflow (*i.e.*, qualitative identifications are made on a pool of succinylpeptides from 9 samples mixed together for which relative quantitative comparisons are made). To explore the latter possibility, we plotted the fold change of all sites of lysine succinylation at 31 weeks (KO/WT) and 15 weeks (KO/WT) in fatty acid oxidation (Fig. 4*E*) and the TCA cycle (Fig. 4*F*). We found that the fold change of at least 50% of succinylation sites on proteins in fatty acid oxidation and the TCA cycle increased from 15 weeks (light red circles) to 31 weeks (dark red circles) post SIRT5 depletion. Only a few SIRT5 succinylation targets have been validated in the heart: lysine 179 and 335 on SDHA (4), and lysine 351 on HDHA (5). When we compare the fold change of these sites at 15 weeks, 31 weeks, and the whole-body SIRT5KO (6) (Fig. 4*G–I*), we find that the $\log_2$ fold-change is about the same in the 31-week and whole-body conditions, but trends lower in the 15-week samples. These data suggest that succinylation of SIRT5 targets may not occur immediately after depletion of SIRT5; indeed, these data suggest that maximal succinylation on validated targets of SIRT5 occurs 31 weeks after *Sirt5* ablation.

Together, our data reveal that deletion of *Sirt5* postnatally in the heart results in accumulation of protein lysine succinylation over the course of several weeks to months, while SIRT5 protein expression is maximally depleted about 3 weeks after *Sirt5* deletion by Cre. These findings provide a novel model to study the effect of loss of SIRT5 under conditions of basal succinylation and/or hypersuccinylation.

Heart specific SIRT5KO mice response to pressure overload induced hypertrophy—In order to determine if the phenotype of increased mortality with pressure overload induced hypertrophy in SIRT5KO mice, compared to WT mice is a cardiomycotye- or whole-body effect of SIRT5 (6), we induced left ventricle cardiac hypertrophy by performing TAC in the heart specific SIRT5KO mice. In this study, fl/fl control mice and fl/fl;MCM mice were fed a tamoxifen diet for 8 days immediately after weaning. The mice were fed a regular chow diet for 14 weeks in order to normalize any effects of Cre toxicity and to age match the animals in the whole body SIRT5KO TAC study. TAC surgery was performed on all animals in the study and serial echocardiograms were taken at 0-, 2-, 4-, 8-, 12-, and 16-weeks to investigate cardiac morphology and function (Fig. 5*C*). The most striking phenotype in whole-body SIRT5KO mice we previously reported was decreased survival over the course of 16 weeks of TAC. We repeated this study in the fl/fl and fl/fl;MCM mice and, to our surprise, did not observe a difference in the survival between the two groups with TAC (Fig. 5*B*). Within the first week, there was overall 30% mortality which was likely due to surgery (~20% mortality is expected with TAC). Over the remaining 15 weeks of observation, there was only one instance of mortality in each group. At the end of 16 weeks, gradients were measured on surviving mice and both groups had gradients well above the accepted 20 mmHg cut-off (data not shown). Wall thickness significantly increased in fl/fl and fl/fl;MCM groups (compared to their respective pre-TAC wall thickness) within

the first two weeks of TAC (Fig. 5*C*), indicative of the development of hypertrophy. However, we observed no difference between genotypes. LV weight-to-body weight was measured at the end of the study (data not shown) and no differences in genotype were observed. Additionally, we observe that cardiac function is maintained over the course of this TAC study as fractional shortening is not significantly changed over time or between genotypes (Fig. 5*D*). These morphological and functional changes are consistent with the development of left ventricle hypertrophy with no apparent cardiac dysfunction. Together, these data show that the phenotype observed in the whole body SIRT5KO mouse of increased mortality compared to WT controls with TAC does not repeat in the inducible, heart-specific SIRT5KO mouse model under these conditions.

Effect of pressure overload induced hypertrophy on metabolism and protein lysine succinylation—Although we saw no differences in cardiac function by measurements of fractional shortening, we probed the possibility that there could be a molecular signature of a trajectory towards cardiac dysfunction as we observed in the whole-body SIRT5KO heart under TAC stress (6). We examined the metabolite profiles of fl/fl and fl/fl;MCM hearts isolated from mice before and after 16 weeks of TAC by using high resolution mass spectrometry. and saw no differences in metabolite profiles between genotypes in either the pre-TAC (Fig. 6*A*) or post-TAC (Fig. 6B) group. This suggests that cardiac metabolic pathways between WT and heart-specific SIRT5KO are similar under both basal and post-TAC conditions. In contrast, we saw evidence of reduced oxidative metabolism via metabolic profiling in the whole-body SIRT5KO mouse heart compared to WT heart after 4 weeks of TAC (6). To further investigate the possibility of differential cardiac energetics between genotypes, we examined the ratio of PCr/ATP, lactate/pyruvate, and β-hydroxybutyrate/acetoacetate (Fig. 6*C-E*). We found no differences in these ratios in either the pre-TAC or post-TAC groups. Interestingly, the β-hydroxybutyrate/acetoacetate was significantly increased under the TAC condition, suggesting that oxidative metabolism may be increased in the post-TAC condition, consistent with the development of cardiac hypertrophy and maintenance of cardiac function. Additionally, mRNA expression of genes that regulate cardiac metabolism were the same in the fl/fl and fl/fl;MCM mice after TAC (Fig. 6*F*), providing further evidence of no additional effect of TAC on metabolism in the heart-specific SIRT5KO mice compared to their littermate controls.

Given the surprisingly similar metabolite profiles in the fl/fl and fl/fl;MCM hearts, we decided to interrogate the effect of TAC surgery (and development of left ventricle hypertrophy) on protein lysine succinylation. In the whole-body SIRT5KO heart, succinylation decreased in the 4-week post-TAC, compared to pre-TAC SIRT5KO animals (6). A decrease in succinylation over the course of a 16-week study could explain the similar metabolite profiles. However, we found that protein succinylation was 2-fold higher in fl/fl;MCM mice, compared to fl/fl mice in the pre-TAC group, and that protein succinylation was 4-fold higher in fl/fl;MCM mice, compared to fl/fl mice in the post-TAC group (Fig. 6*G–H*). Additionally, there was an increase in protein succinylation when comparing the fl/fl;MCM 16-week post- TAC group and fl/fl;MCM pre-TAC group (Fig. 6*G–H*). In contrast to whole-body SIRT5KO mice where protein succinylation decreases with 4 weeks of TAC, we find that succinylation increases with 16 weeks of TAC in heart-specific SIRT5KO mice. In both models, there is no change in succinylation with TAC in the control groups (sWT or fl/fl). SIRT5 protein expression was the same in the fl/fl;MCM pre-TAC and 16-week TAC groups (Fig. 6*G* and *I*). Thus, there is a difference in protein succinylation in the whole-body SIRT5KO mouse model and heart-specific SIRT5KO mouse model both at the time of TAC surgery and in response to TAC although *Sirt5* is ablated in the heart in both models. Together, these data suggest that the phenotype observed in the whole-body SIRT5KO mouse model with TAC may be influenced by a role of SIRT5 in tissues outside the heart and is likely not a direct effect of the accumulation of lysine succinylation on cardiac proteins in adulthood.

DISCUSSION

A major goal of this study was to determine if increased mortality in whole-body SIRT5KO mice exposed to pressure overload induced cardiac hypertrophy was a cardiac-intrinsic or an effect of SIRT5 in extra-cardiac tissues. In order to answer this question, we developed a novel, tamoxifen-inducible, cardiomyocyte specific SIRT5KO

mouse model and characterized the cardiac succinylome. Similar to our previous study (6), we used TAC surgery to initiate cardiac hypertrophy by pressure overload.

To our knowledge, prior studies involving tissue-specific sirtuin KO mouse models have not been inducible but driven by constitutive expression of Cre. A study characterizing a liver-specific SIRT3KO mouse model and a skeletal-muscle-specific SIRT3KO mouse model reported similar acetylation profiles compared to the whole body SIRT3KO mouse model (10). In contrast, in the heart specific SIRT5KO mouse model, we find that succinylation accumulates over a time course of months after *Sirt5* ablation, with no change in succinylation in fl/fl controls after feeding the tamoxifen diet (Fig. 2).

One emerging model suggests that acylation is a form of carbon stress and that sirtuins function to remove acyl-lysine modifications as a part of the protein quality-control network (20). Acylation could occur non-enzymatically, and recent studies from our lab demonstrate that succinyl-CoA undergoes intramolecular catalysis to form a highly reactive cyclic anhydride intermediate (21). In support of this notion, incubating cell protein lysates *ex vivo* with increasing concentrations of acyl-CoA's increases the acyl-lysine signal as measured by Western blot (22). Our observations here suggest that accumulation of succinylation in this model is a result of availability of reactive succinyl-CoA coupled with the loss of SIRT5, the only known lysine desuccinylase. Given the reactive anhydride that forms during intramolecular catalysis of succinyl-CoA and the extended length of time to see any observable differences in lysine succinylation after SIRT5 depletion, we predict that the succinyl-CoA available for protein lysine succinylation would be relatively low in abundance under basal conditions. Previous studies have shown that acetylation accumulates under disease conditions such as heart failure when acetyl-CoA homeostasis is altered (23). To further test this model of succinylation in the heart-specific SIRT5KO mouse model, it would be of interest to increase succinyl-CoA concentrations and determine the effect on the time of increases in protein lysine succinylation.

Inducible, heart-specific SIRT5KO mice were exposed to chronic pressure overload *via* TAC surgery for 16 weeks in order to determine if this mouse model recapitulated the whole-body SIRT5KO mouse model's response to the same stress. Previously, we described a potential mechanism of increased mortality due to impaired oxidative metabolism in cardiomyocytes, with a primary lesion at OXPHOS, and an accelerated trajectory of cardiac dysfunction (6). Surprisingly, we saw no difference in mortality between heart-specific SIRT5KO mice and their littermate controls in response to TAC. Additionally, we observed no differences in cardiac hypertrophy or function between genotypes (Fig. 5). This was in contrast to the whole-body SIRT5KO TAC mouse model where we observed an exaggerated hypertrophy compared to WT TAC mice. The exaggerated hypertrophic response to TAC in SIRT5KO mice was based on echocardiogram readings of wall thickness, although we did not observe any genotypic differences in left ventricle weight at the end of the TAC study. We interpreted these data at the time as indicative of two different morphologies of cardiac hypertrophy—the SIRT5KO mice developed primarily concentric hypertrophy while the WT controls developed a mix of concentric and eccentric hypertrophy. Considering the observations made in the heart specific SIRT5KO model in response to TAC, we re-examined the whole-body SIRT5KO echocardiogram data and consider that another interpretation of this data could be pseudo-hypertrophy based on a multi-tissue effect of SIRT5 that effects echocardiogram readings. Physiological factors including heart rate, preload, and afterload combined with environmental factors such as stress and can influence echocardiogram readings (24). Preload can be changed by dehydration (resulting in a lower blood volume) and could also cause the impression of hypertrophy (25). Regardless of this new interpretation of the exaggerated hypertrophy in whole-body SIRT5KO mice in response to TAC, reduced survival in whole-body SIRT5KO compared to WT controls in response to TAC was the most salient finding from this previous study and is clearly not repeated in the inducible, heart-specific SIRT5KO model. One major caveat of this study was the differences in degree of succinylation in the heart-specific SIRT5KO mouse at time of TAC surgery (Fig. 6) compared to the degree of succinylation in the whole-body SIRT5KO mouse at time of TAC surgery. Based on these data, we

consider two models to describe the effect of SIRT5 on cardiac function.

One model that could explain the different response to TAC in the whole-body and heart-specific SIRT5KO models is that the effect is due to a whole-body or multi-tissue role of SIRT5. Although succinylation increases dramatically in the heart in whole-body SIRT5KO mice, it also increases greatly in the kidney, brain, and brain adipose tissue. Cardiac function is intricately linked to kidney function, and thus, increased mortality with TAC in whole-body SIRT5KO mice could be a result of *Sirt5* ablation in both the heart and kidney. Indeed, SIRT5 plays a role in regulating ammonia production by desuccinylation (and activation) of glutaminase whereby loss of SIRT5 leads to increased ammonia production in hepatic and extra-hepatic tissues (26). Increased ammonia production can contribute to kidney disease (27), and could play a role in the response of whole-body SIRT5KO mice to TAC. Additionally, the cardiac hypertrophic response is not exclusive to cardiomyocytes, but also includes an inflammatory response with the infiltration of macrophages and increased fibrosis (28). A role for SIRT3 in preventing fibrosis by activity in fibroblasts has recently been described (14) and several studies suggest that sirtuins may reduce inflammation (29). The specific role of SIRT5 in the inflammatory response is a nascent area of investigation, but recent studies suggests that SIRT5 suppresses the pro-inflammatory response in macrophages (30). Therefore, a possible explanation for lack of difference in response to TAC in cardiomyocyte-specific SIRT5KO mice, compared to WT controls, could be a reduced inflammatory response in non-cardiomyocyte tissues such that is not suppressed in whole-body SIRT5KO mice with TAC; this hypothesis needs to be tested directly.

In another model, we predict that the degree of succinylation may influence the response to TAC. Given the differences in succinylation at the time of TAC surgery in the whole-body SIRT5KO model (6) and the heart-specific SIRT5KO model, it is possible that succinylation of enzymes is not sufficient to alter overall oxidative metabolism in response to TAC. Indeed, we observe no differences in metabolite profiles or metabolic representations of cardiac energetics between fl/fl and fl/fl;MCM after 16 weeks of TAC (Fig. 6). However, when we look at specific targets of SIRT5 in the heart, it appears that succinylation continues to increase between 15-weeks and 31-weeks post SIRT5 depletion (Fig. 4). To address this caveat, mice could be aged for more than 30 weeks after *Sirt5* ablation before TAC surgery in order to increase protein lysine succinylation. However, this would increase the age of the mouse at time of surgery from 12-20 weeks to close to 40 weeks of age. This itself could pose problems in comparing the heart-specific and whole-body models of the same age as whole-body SIRT5KO mice aged to 39 weeks exhibit cardiac dysfunction, compared to controls (5).

Together, these data point to a role of SIRT5 and protein succinylation in the developing heart, either prenatally or early post-natal development. Importantly, a key difference in this cardiomyocyte-specific SIRT5KO model compared to the whole-body SIRT5KO model is the time when *Sirt5* is ablated. In the whole-body SIRT5KO mouse, *Sirt5* is ablated in the germline and thus the protein is never present in the developing mouse. In contrast, *Sirt5* was ablated at 3 weeks post-birth in the heart-specific SIRT5KO mouse model described here. Our data show that depletion of SIRT5 protein took a number of weeks even after gene ablation. As a result, succinylation was maximally increased in the whole-body SIRT5KO mouse heart compared to WT controls at the earliest time points we tested (6 weeks of age, data not shown), but succinylation was not maximal in the heart-specific SIRT5KO model until 30 weeks after *Sirt5* ablation. This observation provides insight into the kinetics of succinylation and suggests that free succinyl-CoA available for succinylation could be different (in amount, localization, etc.) in the developing heart compared to the adult heart. As a result, it takes several weeks for the highly reactive succinyl-CoA to succinylate available lysine residues. In the heart-specific SIRT5KO model, SIRT5 is present and succinylation is at baseline levels during embryogenesis and early post-natal development, but depleted in early adulthood, the cardiac stress of chronic pressure overload does not result in increased mortality compared to controls. In contrast, in whole-body SIRT5KO model, *Sirt5* is ablated from the germline, and the stress of chronic pressure overload results in increased mortality compared to WT controls. While we suggest some ways that this could be due to a multi-tissue effect

of SIRT5, it will be important to test the effect of SIRT5 in the prenatal heart by using a non-inducible heart-specific SIRT5KO mouse model. Conversely, an inducible, whole-body SIRT5KO model would be informative. Together, these models would certainly provide insight into the role of cardiac succinylation and SIRT5 in the heart.

From this study we conclude that the phenotype of increased mortality with chronic TAC in whole-body SIRT5KO mice does not translate to heart-specific SIRT5KO mice when ablation of *Sirt5* is induced three weeks postnatally. Given the differences in these models, specifically the time of cardiac SIRT5 depletion and subsequent hypersuccinylation, future studies are required to determine the role of SIRT5 in the developing heart. These studies will be focused on understanding the kinetics of *Sirt5* ablation and succinylation in the developing heart, how it influences the response to cardiac stress, and will further clarify the role of SIRT5 as an emerging regulator of survival under cardiac stress.

EXPERIMENTAL PROCEDURES

Animals—All animal research has been reviewed by the Duke University Institutional Animal Care and Use Committee and approved under protocol registry number A091-17-04. To generate the tamoxifen-inducible cardiomyocyte-specific SIRT5KO mouse, we crossed $SIRT5^{fl/fl}$ females (18) (generous gift from Johan Auwerx, EPFL, Lausanne, Switzerland) with αMHC-$MerCreMer^{+/-}$ (obtained from Jackson Laboratory, Bar Harbor, ME; stock #005657) males to generate littermates with the following genotypes: $SIRT5^{fl/fl}$; αMHC-$MerCreMer^{-/-}$ (hereto referred to as fl/fl) and $SIRT5^{fl/fl}$; αMHC- $MerCreMer^{+/-}$ (hereto referred to as fl/fl;MCM). Additionally, the floxed alleles were crossed out of this line by crossing $SIRT5^{fl/fl}$; αMHC- $MerCreMer^{+/-}$ males with C57BL/6J females from Jackson Laboratory (Bar Harbor, ME, stock #000664) to generate a line of non-floxed αMHC- $MerCreMer^{-/-}$ and αMHC-$MerCreMer^{+/-}$ mice to generate αMHC-$MerCreMer^{+/-}$ (hereto referred to as MCM) mice to control for Cre toxicity. All of these mice are on the C57BL/6J background. Mice were group-housed on a 12-hour light/dark cycle with free access to water and PicoLab Rodent Diet 20 (LabDiet #5053, St. Louis, MO). To induce MerCreMer expression, tamoxifen citrate diet (Envigo Tekland Diets, Madison, WI; TD.130860) was fed for 8-10 days. Tamoxifen citrate pellets were moistened to encourage eating and regular chow was fed over the weekends (after 3-5 days of tamoxifen citrate feeding) to decrease weight loss with new diet. Age, sex, genotype, and number of animals used per study are provided in the corresponding figure legends. All *in vivo* procedures were performed on healthy animals in accordance with the Duke Institutional Animal Care and Use Program.

Western Blots—Left ventricle tissue (whole or part) was dissected and flash frozen. Tissue was homogenized in RIPA buffer with protease inhibitors using a rotor. A Teflon pestle rotated at 1000 rpm was used to homogenize tissues with approximately 10 strokes. Tissue was spun down for 10 minutes at 10,000 x g at 4 °C. The supernatant was collected and a BCA assay (Sigma) was run to determine protein concentration. Protein concentrations for each sample were normalized to 2 µg/µL in 4X Laemmli Sample Buffer (Bio-Rad). Whole-cell protein extracts were resolved by SDS-PAGE using stain free Bio-Rad gels and transferred to nitrocellulose membranes using Bio-Rad's Trans- Blot Turbo. Total protein was quantified with the Gel Doc XR^{+} (Bio-Rad) using stain free technology. The membranes were blocked in 5% milk in TBS-T (TBS containing 0.1% Tween 20) for 1 hour at room temperature and probed with primary antibodies in TBS- T. For anti-acyl-K blots, 3% BSA was added to the primary antibody solution. After incubation with infrared dye-conjugated antibodies, the blots were developed using the Odyssey Infrared Imaging System (LI-COR Biosciences). Commercial antibodies were used as follows: anti-Succinyl-K from PTM (401). Anti-SIRT5 was provided as a generous gift from Leonard Guarente (MIT, Cambridge, MA).

RT-qPCR—Animals were euthanized by exposure to CO2 for 5 minutes and immediate excision of the whole heart. Heart was washed in PBS and the left ventricle was dissected. A small (approximately 50 mg) piece of the left ventricle apex was flash frozen immediately for downstream RNA analysis. RNA was extracted from tissues using RNeasy Mini Kit from Qiagen (74106). cDNA was made from 750 ng RNA using iScript cDNA Synthesis Kit from Bio-Rad (170-8890) and diluted 1:8 with nuclease free water. Amplification was performed using iTaq Universal SYBR Green

Supermix from Bio- RAD (1725121) on the QuantStudio 6 Flex (ThermoFisher Scientific). RT-qPCR reaction mix contained 2.5 µL 1:8 cDNA, 0.5 µL of 10 µM forward and reverse primer mix, 4 µL SYBR, and 1 µL nuclease free water. *36B4* was used as a reference gene and relative expression was calculated using the $^{\Delta\Delta}$CT method.

Proteomics: Protein Digestion—Animals were euthanized by exposure to CO_2 for 5 minutes and immediate excision of the whole heart. Heart was washed in PBS and the left ventricle was dissected and immediately flash frozen. Left ventricle tissue was pulverized using a Bessman Tissue Pulverizer (Spectrum Labs) in liquid nitrogen and approximately 20 mg of tissue was weighed out for further sample preparation. To each sample, 300 µL of urea lysis buffer (8 M urea, 50 mM pH 8.0 Tris, 40 mM NaCl, 2 mM $MgCl_2$, 10 mM nicotinamide, 10 µM TSA, protease inhibitors (Roche cOmplete Ultra)) was added and the tissue was disrupted with a TissueLyzer (Qiagen) for one minute at 30 Hz. Samples were frozen on dry ice and thawed at 32 °C for three freeze-thaw cycles. Samples were sonicated with a pencil-tip probe sonicator at power level 3, 3 bursts for 5 seconds each. Samples were centrifuged at 10,000 x g for 10 minutes at 4 °C. Supernatant was placed in clean tube and BCA assay (Sigma) was performed to determine protein concentration, after which 500 µg of each sample were diluted in 200 µL urea lysis buffer. Samples were reduced by adding 5 mM dithiothreitol (DTT) and incubating at 32 °C for 30 minutes, cooled to room temperature (RT) and alkylated by incubation with 15 mM iodoacetamide (IAM) for 30 minutes at RT in the dark. This reaction was quenched by adding DTT to a final concentration of 15 mM. To each sample, 5 µg of LysC (Wako) was added and digestion proceeded for four hours at 32 °C. Samples were subsequently diluted to 1.5 M urea and 10 µg sequence grade trypsin (Promga) was added. Samples were digested overnight at 32 °C. Samples were acidified to 0.5% v/v trifluoroacetic acid (TFA), spun down at room temperature, and de-salted using a 50 mg tC18 Sep-Pak SPE column (Waters). Samples were dried using a Speed Vac.

Proteomics: Peptide Isobaric Labeling—Samples were resuspended in 100 µL of 200 mM triethylammonium bicarbonate (TEAB). Labeling reagents (Thermo TMT10plex Kit, 90110) were resuspended in 50 µL acetonitrile (ACN) and subsequently added to the sample tubes to incubate for four hours at RT while shaking. Reactions were quenched by adding 0.8 µL of 50% hydroxylamine and shaking for 15 minutes at RT. All samples were combined into a single tube, which was vortexed, and dried in a Speed Vac. The sample was re-constituted in 0.5% TFA and desalted on a 100 mg tC18 Sep-Pak SPE column (Waters), and eluted. Subsequently, 5% of the "input" material was removed for quantification of unmodified peptides—leaving the remaining 95% in a second aliquot for succinylpeptide enrichment. Both aliquots of the de-salted peptide mixture were dried on a Speed Vac.

Proteomics: Succinylpeptide enrichment—Beads conjugated with succinyl-lysine antibody (CST, PTMscan Succinyl- Lysine Motif, 13764) were washed two times in ice cold PBS. All wash steps include spinning the bead slurry down at 2,000 x g at 4 °C for 30 seconds and carefully removing the supernatant. Beads were transferred to a new tube and washed two more times with ice cold PBS. TMT-labeled sample (the larger aliquot from above containing 95% of the peptide mixture) was resuspended in 1.4 mL 1X IAP buffer (CST, PTMscan Succinyl-Lysine Motif, 13764) and centrifuged at 10,000 x g at 4 °C for 5 minutes. The supernatant was added to the washed succinyl-lysine antibody beads and incubated on a rotator overnight at 4 °C. The sample was centrifuged at 2,000 x g at 4 °C for 30 seconds and the flow-through was saved. The beads were washed two times with 1X IAP with gentle mixing by inversion in between washes. Beads were washed three times with milli-Q H2O and transferred to a new tube. Succinyl peptides were eluted from the beads by adding 100 µL of 0.15% TFA and letting sit at room temperature for 10 minutes with gentle mixing every 2-3 minutes. Sample was centrifuged at 2,000 x g for 30 seconds and supernatant transferred to new tube. This elution step was repeated once and sample was brought to a final concentration of 0.5% TFA. Sample was cleaned by loading and eluting from a 50 mg tC18 Sep-Pak SPE column (Waters). Sample was dried on a Speed Vac. Sample was resuspended in 22.5 µL0.1% formic acid (FA), loaded into an auto-sampler tube, and stored at -80°C until ready for mass spec analysis.

Proteomics: Input fractionation—Input sample was resuspended in 0.5 mL of 0.1% TFA and diluted to 0.33 mg/mL in 0.1% TFA.

Fractionation columns (Pierce, High pH Reversed-Phase Peptide Fractionation Kit, 84868) were conditioned according to the manufacturer's instructions and 300 µL of sample was loaded onto a fractionation column and centrifuged at 3,000 x g for 2 minutes at RT. Sample was washed with 300 µL water followed by 300 µL of 5% ACN, 0.1% TFA. Sample was eluted in 8 fractions containing increasing amount of ACN. Fractions were dried in Speed Vac. Sample fractions were resuspended in 10 µL of 0.1% FA. Peptide fractions were quantified using Pierce Quantitative Colorimetric Peptide Assay (Thermo Scientific, 23275).

Proteomics: Nano-LC-MS/MS—All samples were subjected to *nano*LC-MS/MS analysis using an EASY-nLC UPLC system (Thermo Fisher Scientific) coupled to a *Q Exactive Plus* Hybrid Quadrupole-Orbitrap mass spectrometer (Thermo Fischer Scientific) *via* an EASY-Spray nanoelectrospray ionization source (Thermo Fischer Scientific). Prior to injection, the succinylpeptide sample was resuspended in 22.5 µL 0.1% FA and each of the HPRP fractions of the input material were resuspended in enough 0.1% FA to achieve a peptide concentration around 0.15 ug/uL (which was determined precisely using the peptide quantitation assay described above). The succinylpeptide sample was analyzed with technical triplicate runs, with 6.5 µL of sample injected for each. The 8 input HPRP fractions were analyzed in singlicate, with 1 ug injections (roughly 7 µL for each based on the precise concentration). For each injection, the sample was first trapped on an Acclaim PepMap 100 C18 trapping column (3 um particle size, 75 µm × 20 mm) with 18 µL of solvent A (0.1 % FA) at a variable flow rate dictated by max pressure of 500 Bar, after which the analytical separation was performed over a 105 minute gradient (flow rate of 300 nL/minute) of 5 to 40% solvent B (90% ACN, 0.1% FA) using an Acclaim PepMap RSLC C18 analytical column (2 um particle size, 75 µm × 500 mm column (Thermo Fischer Scientific) with a column temperature of 55 ºC. MS^1 (precursor ions) was performed at 70,000 resolution, with an AGC target of $3x10^6$ ions and a maximum injection time of 60 ms. MS^2 spectra (product ions) were collected by data-dependent acquisition (DDA) of the top 10 most abundant precursor ions with a charge greater than 1 per MS1 scan, with dynamic exclusion enabled for a window of 30 seconds. Precursor ions were filtered with a 0.7 m/*z* isolation window and fragmented with a normalized collision energy of 30. MS2 scans were performed at 35,000 resolution, with an AGC target of $1x10^5$ ions and a maximum injection time of 60 ms.

Proteomics: Raw data processing—Raw LC-MS/MS data have been deposited to the ProteomeXchange Consortium via the PRIDE (31) partner repository with the dataset identifier PXD008728. Raw LC-MS/MS data were processed in Proteome Discoverer v2.2 (PD2.2, Thermo Fisher Scientific), using both the Sequest HT (32) and MS Amanda 2.0 (33) search engines. Data were searched against the UniProt mouse complete proteome database of reviewed (Swiss-Prot) and unreviewed (TrEMBL) proteins, which consisted of 52,015 sequences on the date of download (9/23/2017). Default search parameters included oxidation (15.995 Da on M) as a variable modification and carbamidomethyl (57.021 Da on C) and TMT (229.163 Da on peptide N-term and K). To assess labeling efficiency as a quality control measure, the input fraction was re-searched with N-terminal TMT as a variable modification, confirming N-terminal labeling of 88% of all peptide spectral matches (PSMs). Succinyl runs added succinyl (100.01604 Da on K) as a variable modification and changed TMT to a variable modification on K (remaining fixed on peptide N-term). Data were searched with a 10 ppm precursor mass and 0.02 Da product ion tolerance. The maximum number of missed cleavages was set to a default value of 2 (but changed to 4 for succinyl runs) and enzyme specificity was trypsin (full). Considering each data type (succinyl, input) separately, PSMs from each search algorithm were filtered to a 1% false discovery rate (FDR) using the Percolator (34) node of PD2.2. For succinyl data, site localization probabilities were determined for succinyl lysines using the ptmRS algorithm (35). PSMs were grouped to unique peptides while maintaining a 1% FDR at the peptide level and using a 90% site localization threshold for succinyl lysines. Peptides from all samples (succinyl, input) were grouped to proteins together using the rules of strict parsimony and proteins were filtered to 1% FDR using the Protein FDR Validator node of PD2.2. Reporter ion intensities for all PSMs having co-isolation interference below 50% (of the ion current in the isolation window) and average reporter S/N>2.5 were summed together at the

peptide group and protein level, but keeping quantification for each data type (succinyl, input) separate. Peptides shared between protein groups were excluded from protein quantitation calculations.

Proteomics: Statistical analysis—Protein and peptide groups tabs in the PD2.2 results were exported as tab delimited .txt. files, opened in Microsoft EXCEL, and analyzed as described previously (36). First, peptide group reporter intensities for each peptide group in the input material were summed together for each TMT channel, each channel's sum was divided by the average of all channels' sums, resulting in channel-specific loading control normalization factors to correct for any deviation from equal protein/peptide input between each sample. Reporter intensities for peptide groups from the succinyl fraction and for proteins from the input fraction were divided by the loading control normalization factors for each respective TMT channel. Analyzing the acetylpeptide and protein datasets separately, all loading control-normalized TMT reporter intensities were converted to $\log_2$ space, and the average value from the six samples was subtracted from each sample-specific measurement to normalize the relative measurements to the mean. For each genotype-age condition, condition average and standard deviation were calculated. For each genotype comparison (Sirt5 KO vs. control) at each age (15 and 31 weeks) and each age comparison (15 vs. 31 weeks) within each genotype (Sirt5 KO and control), Log_2 fold change, p-value (two-tailed student's t-test, assuming equal variance), and adjusted p-value ($P_{adjusted}$, Benjamini Hochberg FDR correction) were calculated (37, 38). For protein-level quantification, only Master Proteins—or the most statistically significant protein representing a group of parsimonious proteins containing common peptides identified at 1% FDR—were used for quantitative comparison. Succinylpeptide measurements were calculated both alone (referred to as *relative abundance*) and with normalization to any change in the corresponding Master Protein (referred to as *relative occupancy*), calculated by subtracting Log_2 Master Protein values from succinylpeptide quantitation values on a sample-specific basis.

Transverse aortic constriction—Pressure overload in mice was performed by Lan Mao of the Duke Cardiovascular Physiology Core and was induced using methods previously described (39), except that the suture was placed between the left carotid and the left axillary arteries. Serial echocardiography was performed on conscious mice from all groups with a Vevo 2100 high-resolution imaging system (VisualSonics) as previously described.

Metabolite extraction—10 to 20 mg of frozen crushed heart tissue was weighed in an Eppendorf tube and 200 µl of ice cold 80% methanol was added. A glass bead was added and was homogenized using the TissueLyzer for 2 minutes at 30 Hz. 300 µl ice cold 80% methanol was added, vortexed, and incubated on ice for 10 minutes. Tissue extract was centrifuged at 20,000 x g at 4°C for 10 minutes. Supernatant containing 2 mg tissue was transferred to a new Eppendorf tube and dried in vacuum concentrator at room temperature. The dry pellets were reconstituted into 30 µl (per 2 mg tissue) sample solvent (water:methanol:acetonitrile, 2:1:1, v/v) and 3 µl was further analyzed by liquid chromatography-mass spectrometry (LC-MS).

LC-MS method—Ultimate 3000 UHPLC (Dionex) is coupled to Q Exactive Plus-Mass spectrometer (QE-MS, Thermo Scientific) for metabolite profiling. A hydrophilic interaction chromatography method (HILIC) employing an Xbridge amide column (100 x 2.1 mm i.d., 3.5 µm; Waters) is used for polar metabolite separation. Detailed LC method was described previously (40) except that mobile phase A was replaced with water containing 5 mM ammonium acetate (pH 6.8). The QE-MS is equipped with a HESI probe with related parameters set as below: heater temperature, 120 °C; sheath gas, 30; auxiliary gas, 10; sweep gas, 3; spray voltage, 3.0 kV for the positive mode and 2.5 kV for the negative mode; capillary temperature, 320 °C; S-lens, 55; scan range (*m/z*): 70 to 900 for pos mode (1.31 to 12.5 min) and neg mode (1.31 to 6.6 min) and 100 to 1000 for neg mode (6.61 to 12.5 min); resolution: 70000; automated gain control (AGC), 3×10^6 ions. Customized mass calibration was performed before data acquisition.

Metabolomics data analysis—LC-MS peak extraction and integration were performed using commercial available software Sieve 2.2 (Thermo Scientific). The peak area was used to represent the relative abundance of each metabolite in different samples. The missing values were handled as described in previous study (40). Data was

uploaded to Metaboanalyst for further downstream analysis (41, 42).

RT-qPCR—RNA was extracted from tissues using RNeasy Mini Kit from Qiagen (74106). cDNA was made from 750 ng RNA using iScript cDNA Synthesis Kit from BioRad (170-8890). Amplification was performed using iTaq Universal SYBR Green Supermix from BioRAD (1725121) on the QuantStudio 6 Flex (ThermoFisher Scientific). *36B4* was used as a reference gene and relative expression was calculated using the $^{\Delta\Delta}$CT method.

Acknowledgements: We would like to thank Lan Mao and Zhiqiang Chen for their assistance in TAC surgeries and echocardiogram readings. We would like to thank Johan Auwerx, EPFL, Lausanne, Switzerland for the generous gift of the SIRT5$^{fl/fl}$ mice. We would like to thank Howard Rockman, and other members of Kathleen's dissertation committee for feedback. We would also like to acknowledge funding support from the American Heart Association grants 12SDG8840004 and 12IRG9010008, the National Institutes of Health NIA grant R01AG045351, the National Institute of Diabetes, Digestive and Kidney Diseases of the National Institutes of Health under Award Number P30DK096493; KAH is supported by a Ruth L. Kirschstein National Service Research Award F31 Predoctoral Fellowship (1F31HL127959-03) and was supported by an NIH/NIGMS training grant to Duke University Pharmacological Sciences Training Program (5T32GM007105-40); DMA is supported by 1K08HL125905-01. Cardiac phenotyping services were supported by the Edna and Fred L. Mandel Jr. Foundation for Hypertension and Atherosclerosis at Duke.

Conflicts of Interest: The authors declare that they have no conflicts of interest with the contents of this article.

Author Contributions: Conceptualization, KAH, and MDH; Methodology, KAH, JL, and PAG; Investigation, KAH, DMA, JL, and PAG; Writing – Original Draft, KAH and MDH; Writing – Review & Editing, all authors; Supervision, JWL, PAG and MDH; Project Administration, MDH; Funding Acquisition, MDH.

REFERENCES

1. Peng, C., Lu, Z., Xie, Z., Cheng, Z., Chen, Y., Tan, M., Luo, H., Zhang, Y., He, W., Yang, K., Zwaans, B. M. M., Tishkoff, D., Ho, L., Lombard, D., He, T. C., Dai, J., Verdin, E., Ye, Y., and Zhao, Y. (2011) The First Identification of Lysine Malonylation Substrates and Its Regulatory Enzyme. **10**, M111.012658–M111.012658
2. Du, J., Zhou, Y., Su, X., Yu, J. J., Khan, S., Jiang, H., Kim, J., Woo, J., Kim, J. H., Choi, B. H., He, B., Chen, W., Zhang, S., Cerione, R. A., Auwerx, J., Hao, Q., and Lin, H. (2011) Sirt5 is a NAD-dependent protein lysine demalonylase and desuccinylase. *Science*. **334**, 806–809
3. Tan, M., Peng, C., Anderson, K. A., Chhoy, P., Xie, Z., Dai, L., Park, J., Chen, Y., Huang, H., Zhang, Y., Ro, J., Wagner, G. R., Green, M. F., Madsen, A. S., Schmiesing, J., Peterson, B. S., Xu, G., Ilkayeva, O. R., Muehlbauer, M. J., Braulke, T., Mühlhausen, C., Backos, D. S., Olsen, C. A., McGuire, P. J., Pletcher, S. D., Lombard, D. B., Hirschey, M. D., and Zhao, Y. (2014) Lysine glutarylation is a protein posttranslational modification regulated by SIRT5. *Cell Metabolism*. **19**, 605–617
4. Boylston, J. A., Sun, J., Chen, Y., Gucek, M., Sack, M. N., and Murphy, E. (2015) Characterization of the cardiac succinylome and its role in ischemia-reperfusion injury. *J. Mol. Cell. Cardiol.* **88**, 73–81
5. Sadhukhan, S., Liu, X., Ryu, D., Nelson, O. D., Stupinski, J. A., Li, Z., Chen, W., Zhang, S., Weiss, R. S., Locasale, J. W., Auwerx, J., and Lin, H. (2016) Metabolomics-assisted proteomics identifies succinylation and SIRT5 as important regulators of cardiac function. *Proc Natl Acad Sci USA*. 10.1073/pnas.1519858113
6. Hershberger, K. A., Abraham, D. M., Martin, A. S., Mao, L., Liu, J., Gu, H., Locasale, J. W., and Hirschey, M. D. (2017) Sirtuin 5 is required for mouse survival in response to cardiac pressure overload. *Journal of Biological Chemistry*. 10.1074/jbc.M117.809897
7. Dittenhafer-Reed, K. E., Richards, A. L., Fan, J., Smallegan, M. J., Fotuhi Siahpirani, A., Kemmerer, Z. A., Prolla, T. A., Roy, S., Coon, J. J., and Denu, J. M. (2015) SIRT3 Mediates Multi-Tissue Coupling for Metabolic Fuel Switching. *Cell Metabolism*. **21**, 637–646
8. Nishida, Y., Rardin, M. J., Carrico, C., He, W., Sahu, A. K., Gut, P., Najjar, R., Fitch, M., Hellerstein, M., Gibson, B. W., and Verdin, E. (2015) SIRT5 Regulates both Cytosolic and Mitochondrial Protein Malonylation with Glycolysis as a Major Target. *Mol Cell*. 10.1016/j.molcel.2015.05.022
9. Hirschey, M. D., Shimazu, T., Jing, E., Grueter, C. A., Collins, A. M., Aouizerat, B., Stančáková, A., Goetzman, E., Lam, M. M., Schwer, B., Stevens, R. D., Muehlbauer, M. J., Kakar, S., Bass, N. M., Kuusisto, J., Laakso, M., Alt, F. W., Newgard, C. B., Farese, R. V., Jr, Kahn, C. R., and Verdin, E. (2011) SIRT3 Deficiency and Mitochondrial Protein Hyperacetylation Accelerate the Development of the Metabolic Syndrome. *Mol Cell*. **44**, 177–190
10. Fernandez-Marcos, P. J., Jeninga, E. H., Canto, C., Harach, T., de Boer, V. C. J., Andreux, P., Moullan, N., Pirinen, E., Yamamoto, H., Houten, S. M., Schoonjans, K., and Auwerx, J. (2012) Muscle or liver-specific Sirt3 deficiency induces hyperacetylation of mitochondrial proteins without affecting global metabolic homeostasis. *Sci. Rep.* 10.1038/srep00425
11. Pillai, V. B., Sundaresan, N. R., Kim, G., Gupta, M., Rajamohan, S. B., Pillai, J. B., Samant, S., Ravindra, P. V., Isbatan, A., and Gupta, M. P. (2010) Exogenous NAD blocks cardiac hypertrophic response via activation of the SIRT3-LKB1-AMP-activated kinase pathway. *Journal of Biological Chemistry*. **285**, 3133–3144
12. Hafner, A. V., Dai, J., Gomes, A. P., Xiao, C.-Y., Palmeira, C. M., Rosenzweig, A., and Sinclair, D. A. (2010) Regulation of the mPTP by SIRT3-mediated deacetylation of CypD at lysine 166 suppresses age-related cardiac hypertrophy. *Aging (Albany NY)*. **2**, 914–923

13. Martin, A. S., Abraham, D. M., Hershberger, K. A., Bhatt, D. P., Mao, L., Cui, H., Liu, J., Liu, X., Muehlbauer, M. J., Grimsrud, P. A., Locasale, J. W., Payne, R. M., and Hirschey, M. D. (2017) Nicotinamide mononucleotide requires SIRT3 to improve cardiac function and bioenergetics in a Friedreich's ataxia cardiomyopathy model. *JCI Insight*. 10.1172/jci.insight.93885
14. Sundaresan, N. R., Bindu, S., Pillai, V. B., Samant, S., Pan, Y., Huang, J.-Y., Gupta, M., Nagalingam, R. S., Wolfgeher, D., Verdin, E., and Gupta, M. P. (2015) SIRT3 Blocks Aging-Associated Tissue Fibrosis in Mice by Deacetylating and Activating Glycogen Synthase Kinase 3β. *Mol Cell Biol*. **36**, 678–692
15. Sohal, D. S., Nghiem, M., Crackower, M. A., Witt, S. A., Kimball, T. R., Tymitz, K. M., Penninger, J. M., and Molkentin, J. D. (2001) Temporally regulated and tissue-specific gene manipulations in the adult and embryonic heart using a tamoxifen-inducible Cre protein. *Circ. Res.* **89**, 20–25
16. Bersell, K., Choudhury, S., Mollova, M., Polizzotti, B. D., Ganapathy, B., Walsh, S., Wadugu, B., Arab, S., and Kühn, B. (2013) Moderate and high amounts of tamoxifen in αMHC-MerCreMer mice induce a DNA damage response, leading to heart failure and death. *Dis Model Mech*. **6**, 1459–1469
17. Lexow, J., Poggioli, T., Sarathchandra, P., Santini, M. P., and Rosenthal, N. (2013) Cardiac fibrosis in mice expressing an inducible myocardial-specific Cre driver. *Dis Model Mech*. **6**, 1470–1476
18. Yu, J., Sadhukhan, S., Noriega, L. G., Moullan, N., He, B., Weiss, R. S., Lin, H., Schoonjans, K., and Auwerx, J. (2013) Metabolic Characterization of a Sirt5 deficient mouse model. *Sci. Rep.* **3**, 2806
19. Mi, H., Muruganujan, A., Casagrande, J. T., and Thomas, P. D. (2013) Large-scale gene function analysis with the PANTHER classification system. *Nat Protoc*. **8**, 1551–1566
20. Wagner, G. R., and Hirschey, M. D. (2014) Nonenzymatic Protein Acylation as a Carbon Stress Regulated by Sirtuin Deacylases. *Mol Cell*. **54**, 5–16
21. Wagner, G. R., Bhatt, D. P., O'Connell, T. M., Thompson, J. W., Dubois, L. G., Backos, D. S., Yang, H., Mitchell, G. A., Ilkayeva, O. R., Stevens, R. D., Grimsrud, P. A., and Hirschey, M. D. (2017) A Class of Reactive Acyl-CoA Species Reveals the Non-enzymatic Origins of Protein Acylation. *Cell Metabolism*. **25**, 823–837.e8
22. Wagner, G. R., and Payne, R. M. (2013) Widespread and enzyme-independent N{epsilon}-acetylation and N{epsilon}-succinylation in the chemical conditions of the mitochondrial matrix. *Journal of Biological Chemistry*. 10.1074/jbc.M113.486753
23. Horton, J. L., Martin, O. J., Lai, L., Riley, N. M., Richards, A. L., Vega, R. B., Leone, T. C., Pagliarini, D. J., Muoio, D. M., Bedi, K. C., Jr., Margulies, K. B., Coon, J. J., and Kelly, D. P. (2016) Mitochondrial protein hyperacetylation in the failing heart. *JCI Insight*. **1**, 1–14
24. DeMaria, A. N., Neumann, A., Schubart, P. J., Lee, G., and Mason, D. T. (1979) Systematic correlation of cardiac chamber size and ventricular performance determined with echocardiography and alterations in heart rate in normal persons. *Am. J. Cardiol.* **43**, 1–9
25. Di Segni, E., Preisman, S., Ohad, D. G., Battier, A., Boyko, V., Kaplinsky, E., Perel, A., and Vered, Z. (1997) Echocardiographic left ventricular remodeling and pseudohypertrophy as markers of hypovolemia. An experimental study on bleeding and volume repletion. *J Am Soc Echocardiogr*. **10**, 926–936
26. Polletta, L., Vernucci, E., Carnevale, I., Arcangeli, T., Rotili, D., Palmerio, S., Steegborn, C., Nowak, T., Schutkowski, M., Pellegrini, L., Sansone, L., Villanova, L., Runci, A., Pucci, B., Morgante, E., Fini, M., Mai, A., Russo, M. A., and Tafani, M. (2015) SIRT5 regulation of ammonia-induced autophagy and mitophagy. *Autophagy*. **11**, 0–270
27. Chen, W., and Abramowitz, M. K. (2014) Metabolic acidosis and the progression of chronic kidney disease. *BMC Nephrol*. **15**, 55

28. Samak, M., Fatullayev, J., Sabashnikov, A., Zeriouh, M., Schmack, B., Farag, M., Popov, A.-F., Dohmen, P. M., Choi, Y.-H., Wahlers, T., and Weymann, A. (2016) Cardiac Hypertrophy: An Introduction to Molecular and Cellular Basis. *Med Sci Monit Basic Res*. **22**, 75–79
29. Winnik, S., Auwerx, J., Sinclair, D. A., and Matter, C. M. (2015) Protective effects of sirtuins in cardiovascular diseases: from bench to bedside. *Eur. Heart J.* **36**, 3404–3412
30. Wang, F., Wang, K., Xu, W., Zhao, S., Ye, D., Wang, Y., Xu, Y., Zhou, L., Chu, Y., Zhang, C., Qin, X., Yang, P., and Yu, H. (2017) SIRT5 Desuccinylates and Activates Pyruvate Kinase M2 to Block Macrophage IL-1β Production and to Prevent DSS-Induced Colitis in Mice. *CellReports*. **19**, 2331–2344
31. Vizcaíno, J. A., Csordas, A., del-Toro, N., Dianes, J. A., Griss, J., Lavidas, I., Mayer, G., Perez-Riverol, Y., Reisinger, F., Ternent, T., Xu, Q.-W., Wang, R., and Hermjakob, H. (2016) 2016 update of the PRIDE database and its related tools. *Nucleic Acids Research*. **44**, D447–56
32. Yates, J. R. (2015) Pivotal role of computers and software in mass spectrometry - SEQUEST and 20 years of tandem MS database searching. *J. Am. Soc. Mass Spectrom.* **26**, 1804–1813
33. Dorfer, V., Pichler, P., Stranzl, T., Stadlmann, J., Taus, T., Winkler, S., and Mechtler, K. (2014) MS Amanda, a universal identification algorithm optimized for high accuracy tandem mass spectra. *Journal of Proteome Research*. **13**, 3679–3684
34. Käll, L., Canterbury, J. D., Weston, J., Noble, W. S., and MacCoss, M. J. (2007) Semi-supervised learning for peptide identification from shotgun proteomics datasets. *Nature Methods*. **4**, 923–925
35. Taus, T., Köcher, T., Pichler, P., Paschke, C., Schmidt, A., Henrich, C., and Mechtler, K. (2011) Universal and confident phosphorylation site localization using phosphoRS. *J. Proteome Res.* **10**, 5354–5362
36. McDonnell, E., Crown, S. B., Fox, D. B., Kitir, B., Ilkayeva, O. R., Olsen, C. A., Grimsrud, P. A., and Hirschey, M. D. (2016) Lipids Reprogram Metabolism to Become a Major Carbon Source for Histone Acetylation. *CellReports*. **17**, 1463–1472
37. Benjamini, Y., and Hochberg, Y. Controlling the false discovery rate: a practical and powerful approach to multiple testing. *JSTOR*. 10.2307/2346101
38. Lesack, K., and Naugler, C. (2011) An open-source software program for performing Bonferroni and related corrections for multiple comparisons. *J Pathol Inform.* **2**, 52
39. Rockman, H. A., Ross, R. S., Harris, A. N., Knowlton, K. U., Steinhelper, M. E., Field, L. J., Ross, J., and Chien, K. R. (1991) Segregation of atrial-specific and inducible expression of an atrial natriuretic factor transgene in an in vivo murine model of cardiac hypertrophy. *Proc Natl Acad Sci USA*. **88**, 8277–8281
40. Liu, X., Ser, Z., and Locasale, J. W. (2014) Development and quantitative evaluation of a high-resolution metabolomics technology. *Anal. Chem.* **86**, 2175–2184
41. Xia, J., Sinelnikov, I. V., Han, B., and Wishart, D. S. (2015) MetaboAnalyst 3.0--making metabolomics more meaningful. *Nucleic Acids Research*. **43**, W251–7
42. Xia, J., and Wishart, D. S. (2016) Using MetaboAnalyst 3.0 for Comprehensive Metabolomics Data Analysis. *Curr Protoc Bioinformatics*. **55**, 14.10.1–14.10.91

Figures

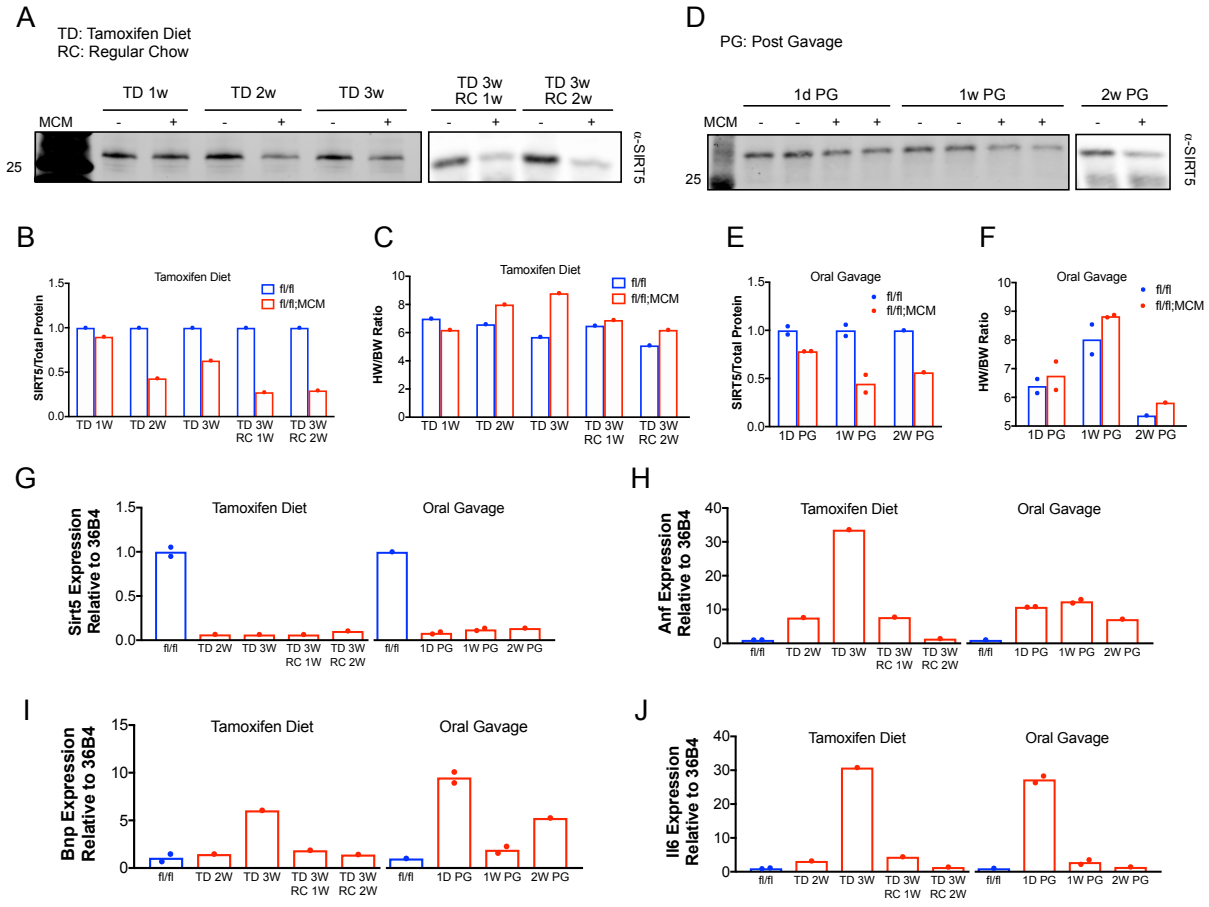

Figure 1: Characterization of tamoxifen-inducible, heart-specific SIRT5KO mouse model.

Tamoxifen diet pilot: (A) Western blot of SIRT5 over time (TD: tamoxifen diet; RC: regular chow; w: week), (B) quantification of blot, (C) heart weight to body weight ratio. Tamoxifen oral gavage pilot: (D) Western blot of SIRT5 over time (PG: post gavage; d: day; w: week), (E) quantification of blot, (F) heart weight to body weight ratio. Blots were normalized to total protein using BioRad stain free technology. Transcript levels of (G) *Sirt5* (H) *Anf* (I) *Bnp* and (J) *Il6* normalized to *36B4* over time in tamoxifen diet (left) and tamoxifen oral gavage (right) pilots. Adult males were used with n=1-2 per group.

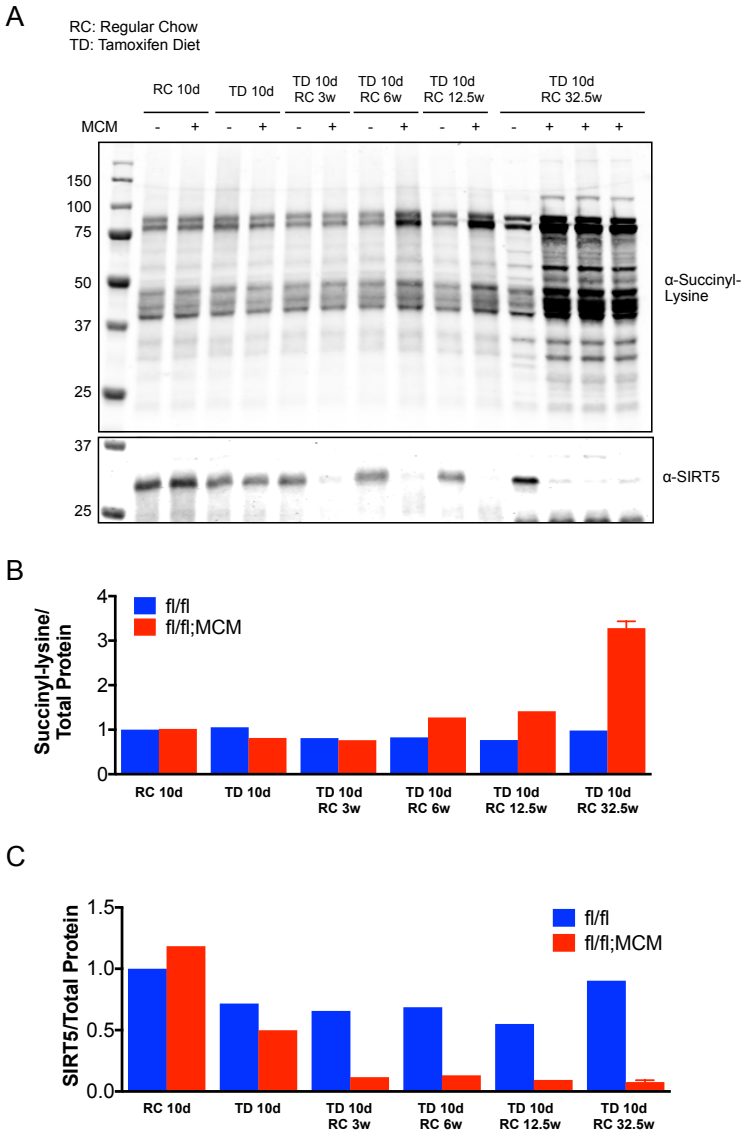

Figure 2: Succinylation accumulates over time after *Sirt5* ablation.

(A) Western blot of protein succinylation and SIRT5 weeks after feeding of tamoxifen diet (RC: regular chow; TD: tamoxifen diet; d: day; w: week). Quantification of (B) succinylation and (C) SIRT5. Blots were normalized to total protein using Bio-Rad stain free technology. Adult females were used in this study with n=1 or 3 per group. Error bars represent SEM.

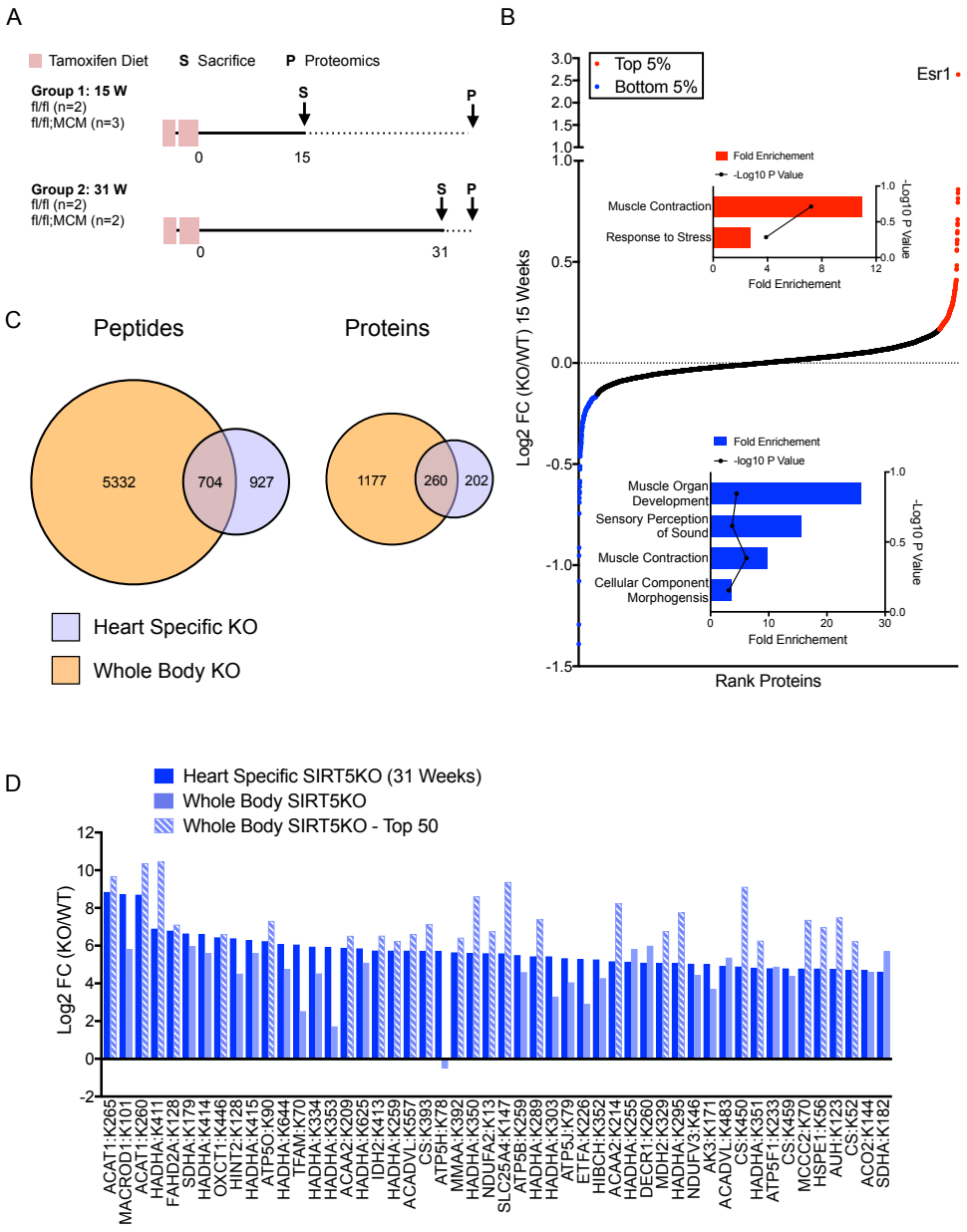

Figure 3: Overview of succinyl proteomics and comparison to whole-body SIRT5KO cardiac succinylome.

(A) Study design. Newly weaned males were fed the tamoxifen diet for 8 days then switched to regular chow for the remainder of the study. Group 1 was sacrificed 15 weeks after tamoxifen feeding, group 2 was sacrificed 31 weeks after tamoxifen feeding. Proteomics on heart tissue from animals in groups 1 and 2 were performed simultaneously. (B) Proteome with proteins ranked according to Log_2FC (KO/WT) at 15 weeks post-tamoxifen feeding. (C) Venn diagrams showing overlap of quantified succinylated peptides and proteins in whole body SIRT5KO succinylome (orange) (6) and heart specific SIRT5KO succinylome (purple). (D) Top 50 highest succinylated peptides identified in heart specific succinylome. Corresponding KO/WT Log2FC in the whole body SIRT5KO is shown in light blue. The shaded light blue bar indicates that it was a top 50 site in the whole body SIRT5KO.

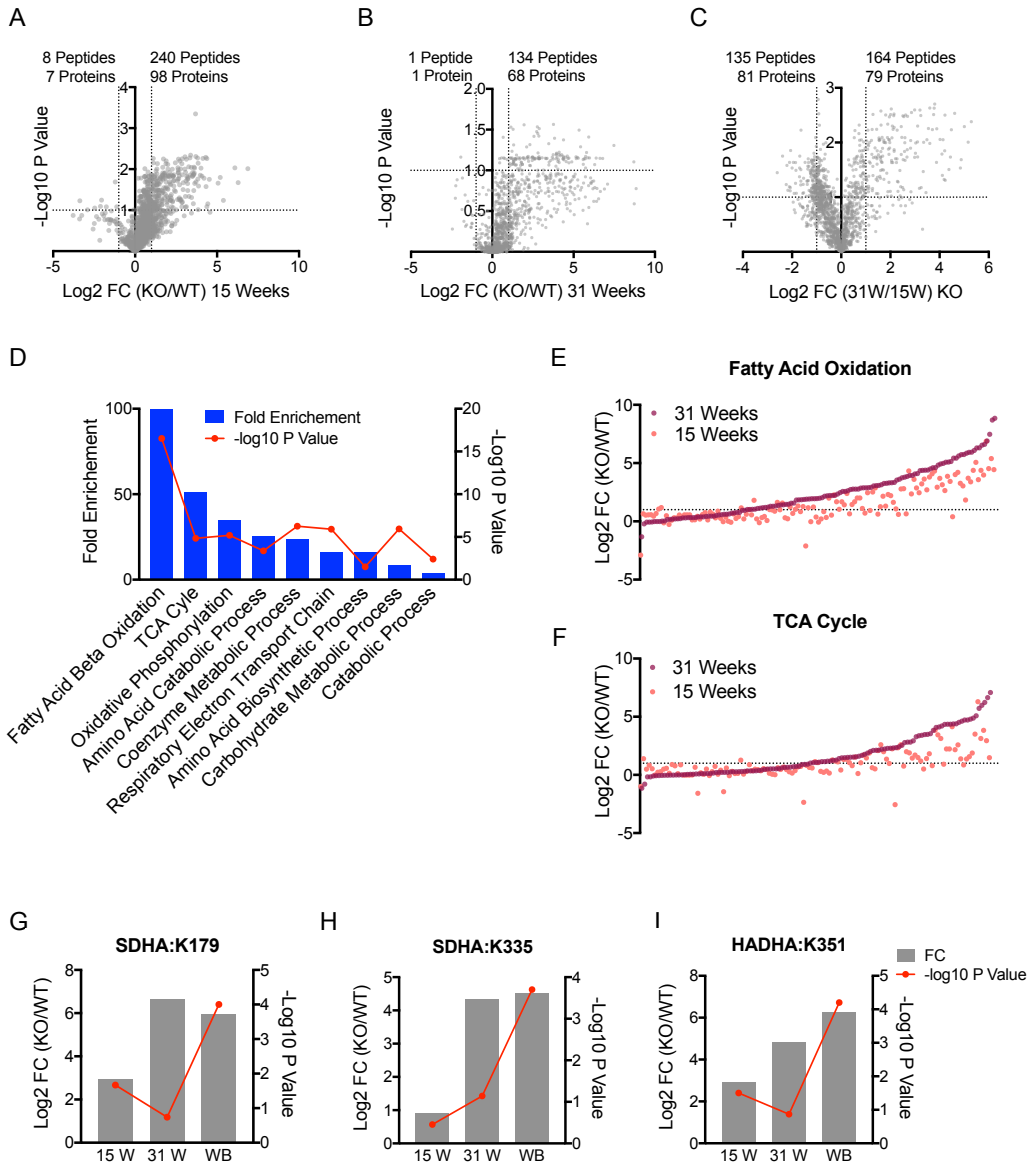

Figure 4: Proteins in pathways of oxidative metabolism are targets of lysine succinylation.

Volcano plots of (A) Log_2 FC (KO/WT) 15 weeks, (B) Log2 FC (KO/WT) 31 Weeks, and (C) Log2 FC (31W/15W) KO. Log_2 FC values are plotted against Benjamini-Hochberg corrected p-values with a 10% FDR. Text indicates the number of peptides and proteins in each group that have decreased succinylation (upper left) and increased succinylation (upper right). (D) Pathway anaylsis of proteins significantly increased in the 31 Week KO to 15 Week KO condition. All sites of lysine succinylation identified in (E) fatty acid oxidation and (F) the TCA cycle. Dark red circles represent the Log_2 FC (KO/WT) 31 weeks-post SIRT5 depletion and light red circles represent the Log2 FC (KO/WT) 15 weeks-post SIRT5 depletion. Sites of lysine succinylation are aligned vertically. Comparison of Log_2 FC (KO/WT) of (H) SDHA:K179, (I) SDHA:K335, and (J) HADHA:K351 in 15 week, 31 week, and whole-body SIRT5KO hearts. P-values are adjusted for multiple comparisons within the same experiment. Data for the whole-body was published in (6).

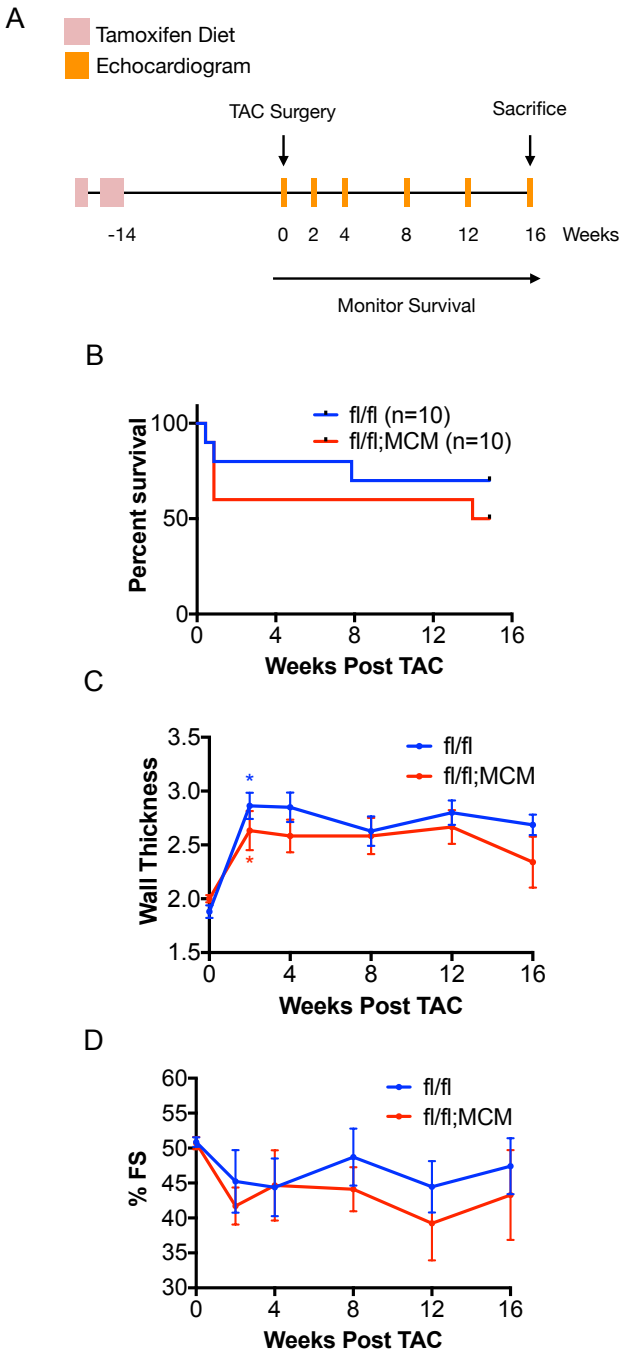

Figure 5: Heart specific SIRT5KO response to pressure overload induced cardiac hypertrophy.

(A) Schematic of study. Males 4-5 weeks of age were fed tamoxifen citrate for 8 days followed by 14.5 weeks of regular chow. Mice were 20-21 weeks of age when TAC surgery was performed. Mice were followed for 16 weeks post TAC. (B) Percent survival (n=10 fl/fl; n=10 fl/fl;MCM). Serial echocardiography was performed at 0-, 2-, 4-, 8-, 12-, and 16-weeks post TAC. (C) Wall thickness (* $p \leq 0.05$, effect of time, two-way ANOVA with multiple comparisons, Bonferroni correction) and (D) Fractional shortening. At end of study n=7 fl/fl; n=5 fl/fl;MCM. Error bars represent mean ± SE.

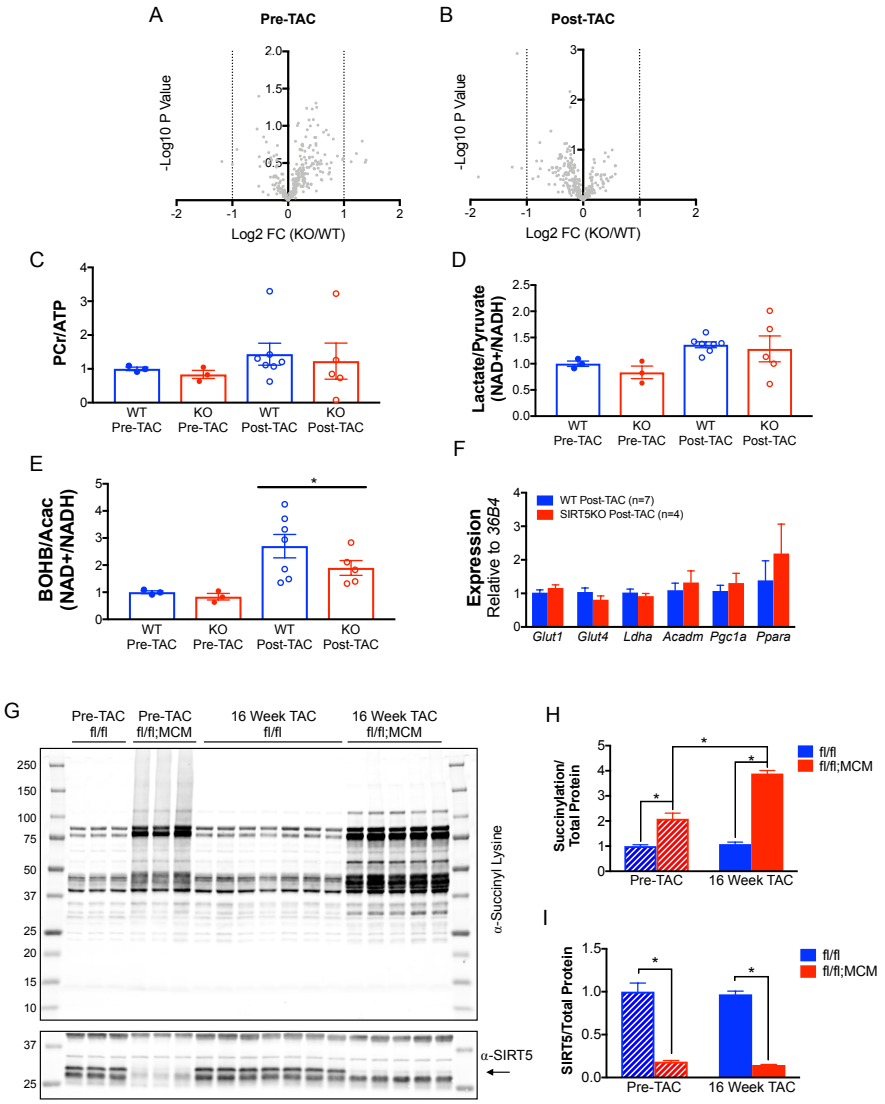

Figure 6: Metabolite profiles between WT and heart-specific SIRT5KO mouse hearts are similar despite differences in protein lysine succinylation.

Males 4-5 weeks of age were fed tamoxifen citrate for 8 days followed by 17.5 weeks of regular chow and were sacrificed (Pre-TAC group; n=3 fl/fl, n=3 fl/fl;MCM). Males 4-5 weeks of age were fed tamoxifen citrate for 8 days followed by 14.5 weeks of regular chow and underwent TAC or sham surgery for 16 weeks and were sacrificed (16 Week TAC group; n=7 fl/fl, n=5 fl/fl;MCM). Volcano plots comparing (A) WT and heart-specific SIRT5KO cardiac metabolites before TAC surgery and (B) after TAC surgery. Uncorrected p-values are represented because Benjamini-Hochberg correction resulted in p-values greater than 1. No metabolites were significantly different with Benjamini-Hochberg correction and a 10% FDR. Ratios of (C) PCr/ATP, (D) Lactate/Pyruvate, and (E) BOHB/Acac. *p≤0.05, effect of TAC, two-way ANOVA. (F) Cardiac mRNA expression of *Glut1*, *Glut4*, *Ldha*, *Acadm*, *Pgc1α*, and *Pparα* in WT (n=7) and heart-specific SIRT5KO (n=4) hearts post-TAC. (G) Western blot of succinylation and SIRT5 pre-TAC and post-TAC. Quantification of (H) succinylation and (I) SIRT5. Blots were normalized to total protein using BioRad stain free technology. Values are mean ± SE. *p≤0.05, two-way ANOVA with multiple comparison, Bonferroni correction.

Ablation of Sirtuin5 in the postnatal mouse heart results in protein succinylation and normal survival in response to chronic pressure overload

Kathleen A Hershberger, Dennis M Abraham, Juan Liu, Jason W. Locasale, Paul A. Grimsrud and Matthew D. Hirschey

J. Biol. Chem. published online May 16, 2018
